# Numerical Modeling of the Flow around a Cylinder using FEATool Multiphysics

**Binahi M. A. Said Ali**
Department of Water Resources Engineering, College of Engineering, Salahaddin University, Iraq
binahi.saidali@su.edu.krd

**Jehan M. Sheikh Suleimany**
Department of Water Resources Engineering, College of Engineering, Salahaddin University, Iraq
jehanmohammed.sheikhsuleimany@su.edu.krd

**Safa S. Ibrahim**
Chemistry Department, Faculty of Science, University of Zakho, Iraq
safa.ibrahim@uoz.edu.krd (corresponding author)

*Received: 17 May 2023 | Revised: 8 June 2023 | Accepted: 9 June 2023*

 *DOI: https://doi.org/10.48084/etasr.6053*

**ABSTRACT**

**The current study examines the numerical analysis of the laminar flow around a cylinder at various Reynolds numbers (0.1, 1.1, 20, 26, 50, 100, and 195). The research found that a steady state can exist for Reynolds number values of 0.1, 1.1, 20, and 26. However, the flow pattern becomes unstable at Reynolds numbers 50, 100, and 195, leading to the development of the Kármán vortex street. The FEATool Multiphysics software in MATLAB (R2019b) was utilized to numerically solve the steady 2D Navier-Stokes equation. The study compared the estimated drag coefficient to previous experimental and analytical studies in Abaqus/CFD. The lift and pressure coefficients were also calculated, and their results were found to be in strong agreement with earlier investigations in terms of predicting pressure and velocity distribution. The analysis provided insight into how the flow field changes with increasing Reynolds numbers.**

***Keywords-drag coefficient; cylinder; FEATool Multiphysics in MATLAB (R2019b); `***

## I. INTRODUCTION

Studies on the flow through a cylinder have been extensive in fields such as fluid mechanics, hydraulics, and wind engineering, as it is crucial to comprehend the dynamic forces that are produced by the flow around an object in determining its aerodynamic shape.

An effective method for gaining a comprehensive understanding of the flow field is by utilizing Computational Fluid Dynamics (CFD), which is widely employed in design processes [1]. In the field of fluid dynamics, the flow around a cylinder has been a topic of interest for numerous researchers [2-4]. Wieselsberger's study [5] verified Lamb's empirical formula and provided extensive experimental data for cylinder flow at both low and high Reynolds number values. The measurements in [6] on a pressurized wind tunnel show that a large circular cylinder experiences a high Reynolds number transition. At Reynolds numbers ranging from $10^6$ to $10^7$, the drag coefficient initially increases from its low supercritical value. However, at $R = 3.5 \times 10^6$, it stabilizes at a value of 0.7. Additionally, beyond this point, the cylinder exhibits clear vortex shedding with a Strouhal number of 0.27. The empirical Reynolds number formulas for the drag coefficient at low Reynolds numbers were summarized in [7]. Authors in [8] used the KPD2 algorithm, an integral method, to determine the boundary layer around a cylinder, correcting distortions in vortex modeling present in earlier versions of the system. Authors in [9] performed a numerical investigation of the velocity and pressure around a cylinder in the near field at Reynolds numbers 100, 500, and 1000. They used the Alternating Direction Implicit (ADI) method to solve the continuity and momentum equations, which describe mass and momentum conservation in the flow field. Authors in [10] applied multi-grid methods to investigate flow past a cylinder at Reynolds number 200. These techniques were used to address the challenge of accurately simulating unstable incompressible flow. The authors validated their solution by comparing it to both numerical and experimental data.

Authors in [11] utilized a two-dimensional (2D) numerical approach combining Reynolds-Averaged Navier-Stokes (RANS) and Large Eddy Simulation (LES) to investigate the flow behavior around a cylinder at high Reynolds numbers. This approach solves Navier-Stokes equations in both stable and unstable flow conditions, as suggested in [12]. To test their

method, authors in [11] studied the flow around a cylinder at low Reynolds numbers using a finite difference and meshless technique, a widely used method in CFD simulations. Authors in [13] employed the finite volume method to analyze the flow through a cylinder in laminar and turbulent regimes by solving the Unsteady Reynolds-Averaged Navier-Stokes (URANS) equations. They used wall interference adjustments to ensure the accuracy of their results in both numerical analysis and experimental investigation. Authors in [14] aimed to control the flow around a circular cylinder by introducing artificial roughness to its exterior, both experimentally and numerically. Using CFD simulations, the researchers determined the correlation between roughness size and Re variations in the Re range of $1\times10^4$ to $2\times10^5$ in a Boundary Layer Wind Tunnel (BLWT). The results were compared with previous experimental data and computational simulations. These findings have practical applications in the testing of scale models in low-speed BLWTs seeking super-critical flow characteristics. Authors in [15] performed a numerical investigation of vortex shedding in laminar flow around two-dimensional (2D) and three-dimensional (3D) circular cylinders using the finite volume method, a commonly used computational fluid dynamics technique. They controlled the flow around high Reynolds number cylinders with surface roughness through analytical and experimental methods. Authors in [16] studied the flow around a round cylinder in a planar channel using 2D and 3D Direct Numerical Simulation (DNS) techniques. They examined the flow behavior at low Reynolds numbers, where vortex shedding was often observed. Similarly, authors in [17] carried out numerical simulations to study the flow through a cylinder in the laminar regime. They employed the finite volume method to solve the Navier-Stokes equations, which describe the conservation of momentum in the flow field. Authors in [18] completed a series of fundamental studies on the fluid flow around a circular cylinder placed in a uniform flow using Abaqus/CFD, a Computer-Aided Engineering (CAE) software package.

Authors in [19] used numerical simulations to study the flow around two oscillating cylinders at a Reynolds number of 100. They applied the characteristic-based-split finite element method and MINI triangular elements to solve the 2D Navier-Stokes equations using an Arbitrary-Lagrangian-Eulerian formulation. The results showed five flow response states via analysis of lift forces, phase portraits, energy transfer, and flow fields for in-phase oscillation at different frequencies and small amplitudes, using power spectra. Authors in [20] carried out experiments on the growth and separation of Leading-Edge Vortices (LEVs) from a plunging profile in a free-surface water tunnel. The experiments measured the direct force and velocity field at a Reynolds number of 10,000, a reduced frequency of 0.25, and a Strouhal number of 0.16, using three different leading-edge shapes. The results showed that the shape of the leading edge significantly impacted the formation of the LEV and the flow pattern. Authors in [21] conducted an experiment to analyze the movement of flow separation points on a circular cylinder at high acceleration rates and Reynolds numbers, using hot-film sensors to measure wall shear stress. The results indicated that as a cylinder accelerates, the flow separation point moves quickly, symmetrically, and linearly from 160° to 85° on both sides. It then fluctuates between 75° and 85° during the rest of the acceleration phase. The pattern of separation points is consistent for both acceleration cases when scaled by non-dimensional time. Authors in [22] conducted research to analyze the flow patterns around a vertical cylinder that rises above the water surface. They employed both experimental and numerical methods to examine the flow under different velocities, with Reynolds and Froude numbers ranging from 15,000 to 60,000 and 0.4 to 1.7, respectively. The findings showed a strong correlation between the experimental and numerical results, particularly in terms of the depth of the cavity downstream of the cylinder, the drag coefficient, and the critical velocity. Authors in [23] focused on using CFD to examine fluid flow around a cylinder. The ANSYS Fluent CFD software was utilized to simulate the flow in both steady and unsteady regimes for specific values of Reynolds number, i.e. 1, 25, 75, and 150. Authors in [24] investigated the effect of a cylindrical object on turbulent flow using numerical simulations with FEATool Multiphysics software. The outcome was evaluated on the basis of pressure differential and drag coefficient and a simulation of turbulent flow past a square cylinder was also performed.

The goal of the current research is to investigate the effect of changing Reynolds number on the flow around a 2D cylinder using FEATool Multiphysics in MATLAB (R2019b). As parts of this study, the drag coefficient, lift coefficient, and pressure coefficient on the cylinder will be calculated and the simulation results will be presented in the form of velocity and pressure contours. After performing the simulations, a thorough analysis of the output will be conducted for each Reynolds number. This configuration allowed the investigation of the influence of the Reynolds number on the flow behavior around the cylinder.

## II. THE SUGGESTED APPROACH

The CFD data generation process is an essential step in the implementation of deep learning algorithms in computational fluid dynamics. The process typically involves the following steps [23]:

- Random obstacle generation: The first step is to generate random obstacles using the MATLAB FEATool solver. This involves defining the geometry of the obstacles and setting up the simulation environment in the software.
- Resolution of the Navier-Stokes equations: The Navier-Stokes equations which describe the behavior of fluid flow, are solved numerically using the immersed method to obtain fluid velocity, pressure, and other flow parameters.
- Acquisition of CFD fluid fields: The final step is to obtain the CFD fluid fields, including the coordinates ($x$, $y$), velocities ($u$, $v$), and pressure ($p$). These fluid fields provide detailed information about the fluid flow patterns and can be used to train deep learning models (Figure 1).

The following sections present the detailed components of the architecture.

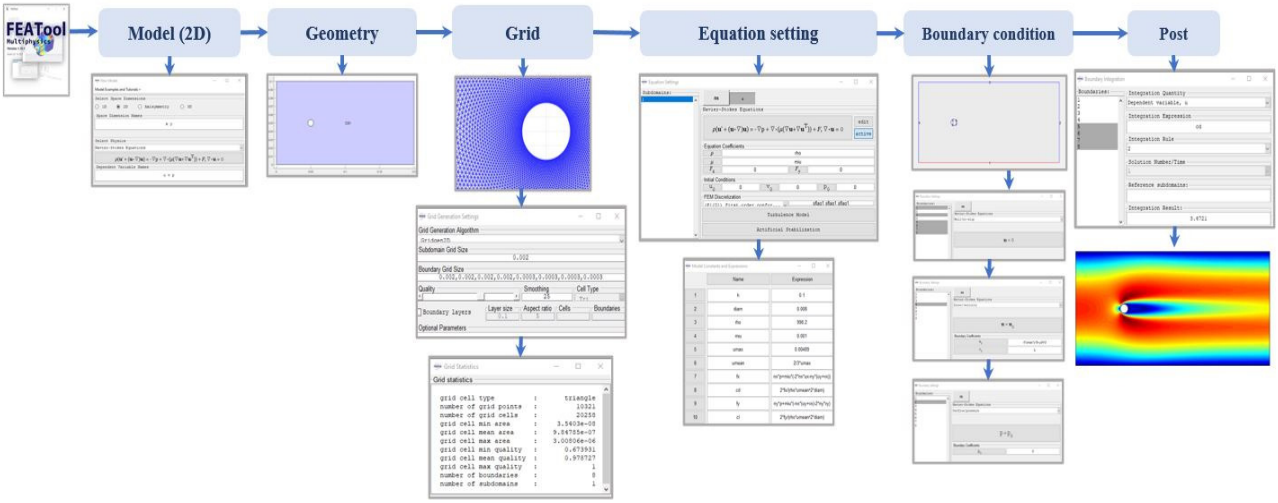


Fig. 1. Data collection from the CFD solver.

### A. Numerical Resolution of the Navier–Stokes Equation

The mass and momentum equations for the incompressible 2D Navier-Stokes system are expressed as follows:

$$\rho\left(\frac{\partial u}{\partial t}+(u.\nabla)u\right)-\nabla.\left(\mu(\nabla u+\nabla u^{T})\right)+p=F \quad (1)$$

$$\nabla.u=0 \quad (2)$$

where the velocity field is denoted by $u$, density is denoted by $\rho$, the pressure field is denoted by $p$, the stress tensor is denoted by $\tau$, $v=\mu/\rho_0$ is the kinematic viscosity, and body forces (ex. gravity) are denoted by $F$, whereas in this case the time dependent term can be neglected. The benchmark quantities that should be computed include the pressure difference between the front and rear of the cylinder $\nabla p = p$ (0.046,0.05) – $p$ (0.054,0.05), and the coefficients of drag $Cd$ and lift $Cl$, defined as:

$$Cd=\frac{2F_d}{\rho U_{mean}^2 D},\ Cl=\frac{2F_l}{\rho U_{mean}^2 D} \quad (3)$$

The drag and lift forces, $F_d$ and $F_l$, can be computed as

$$F_d=\int_S\left(\mu\frac{\partial u_\tau(t)}{\partial n}n_y-pn_x\right)dS \quad (4)$$

$$F_l=-\int_S\left(\mu\frac{\partial u_\tau(t)}{\partial n}n_x-pn_y\right)dS \quad (5)$$

where $u_\tau$ is the velocity in the tangential direction $\tau=(n_y,-n_x,0)^T$.

### B. Random Shape Generation

The numerical simulations for seven different Reynolds numbers ($Re$ = 0.1, 1.1, 20, 26, 50, 100, and 195) were performed using the FEATool Multiphysics simulation toolbox in MATLAB (R2019b), based on previous studies. A rectangular 2D computational domain with a circular cylinder was considered in the numerical domain in the XY plane. Figure 3 presents the benchmark problem for stationary and incompressible laminar flow around a cylinder, which was established in a rectangular 2D domain as in [18]. The dimensions of the rectangular 2D domain were set as: the width in the stream direction is 0.2 m and the height perpendicular to flow is 0.1 m. The cylinder has a diameter of 0.008 m and the center point located at (0.05, 0.05) from the inlet, with the computational domain centered around it, as shown in Figure 2.

### C. Mesh Generation and Boundary Conditions

Grid computation and boundary specification are crucial elements in the execution of CFD modeling. In order to analyze the velocities and pressure fields, a structured mesh with triangular elements of varying sizes was employed during preprocessing and deep learning network training. The fluid domain was divided into two sections, where the region close to the cylinder wall was meshed with elements of a size of 0.0002, and the rest of the fluid domain was meshed with elements of a size of 0.002, as depicted in Figure 3. Consequently, the average number of cells was approximately 35,000.

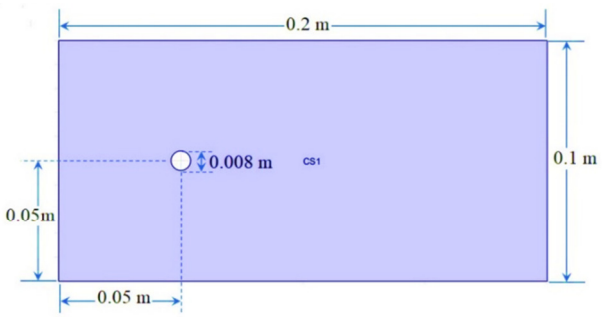


Fig. 2. Geometry of the flow system.

The selection of these element sizes was predicated on the convergence of the drag coefficient, as demonstrated in Figure 4. It was established that a reduction in the grid size below 0.002 did not result in significant alterations to the drag coefficient. Utilizing a structured mesh with strategically chosen element sizes facilitated an exact and efficient simulation of the fluid flow dynamics surrounding the cylinder.

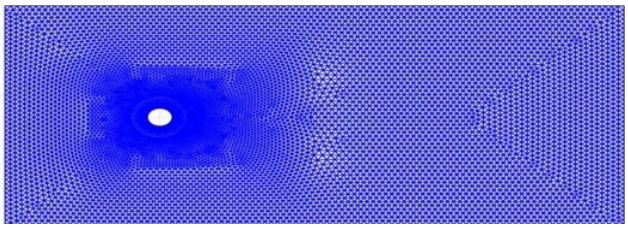

Fig. 3. The structured mesh used to discretize the flow domain around the cylinder, with triangular elements of varying sizes used to capture the complex flow behavior in the boundary layer and far field.

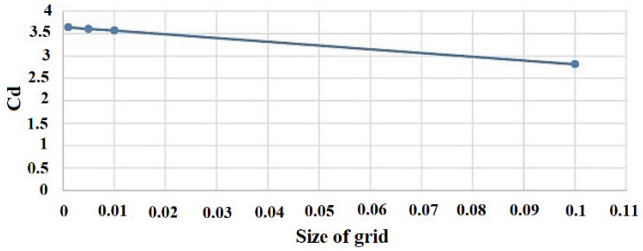


Fig. 4. Variation of the drag coefficient with the size of the grid.

The fluid in this simulation was modeled as a viscous laminar flow. To establish the simulation, it was necessary to input the relevant material properties into the software, as indicated in Table I. These properties included dynamic viscosity and density, both of which are critical for accurately modeling the flow behavior. For boundary setting, the left side of the 2D domain was the velocity inlet and the right side was the pressure outlet. No-slip conditions were assigned to the surface of the circular cylinder and the top and bottom sides as obstacle walls, as illustrated in Figure 5.

TABLE I. PHYSICAL PROPERTIES OF THE FLUID

| Fluid | Density $\rho$ (Kg/m$^3$) | Dynamic Viscosty, $\mu$ ($Pa.s$) |
|---|---|---|
| Water | 998.2 | 0.001 |

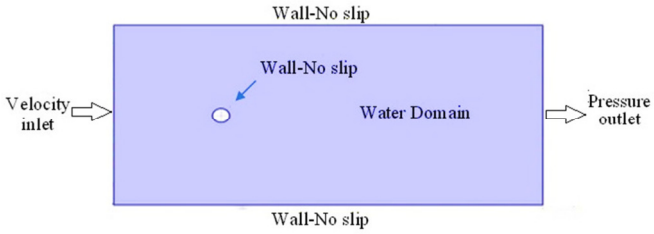


Fig. 5. Boundary specifications for the circulation of water around a cylinder.

In the study of the fluctuation of the flow field at various Reynolds numbers, the inlet velocity input (with $u = u_0$) had its boundary coefficients adjusted seven times based on the Reynolds number through (6)-(8) ($v_0$ was set to 0). The outflow pressure output ($p_0 = 0$) had its boundary coefficient fixed at 0. The walls, with no slip ($u = 0$), did not have any boundary coefficients. Additionally, the boundary conditions were constant, with the density ($\rho$) set to unity at 998.2, viscosity (miu) at 0.001, and a default value of 0 for the forcing term ($F$). The velocity fluctuation was analyzed using the maximum velocity $U_{max}$ and the mean velocity $U_{mean}$, with the Reynolds number ($Re$) representing the laminar flow. The details of the boundary conditions used can be seen in Table II.

$$Re = \frac{\rho U_{mean} D}{\mu} \quad (6)$$

$$U_{max} = \frac{3}{2} U_{mean} \quad (7)$$

$$u = 4yU_{max}\left[\frac{h-y}{h^2}\right] \quad (8)$$

where $u$ represents the entrance velocity (m/s), and $D$ represents the cylinder diameter (m).

TABLE II. MEAN VELOCITY FOR EACH REYNOLDS NUMBER

| Cases | *Re* | $U_{mean}$ (m/s) | $U_{max}$ (m/s) |
|---|---|---|---|
| Case 1 | 0.1 | 0.0000125 | 0.0000188 |
| Case 2 | 1.1 | 0.0001377 | 0.0002066 |
| Case 3 | 20 | 0.0025045 | 0.0037568 |
| Case 4 | 26 | 0.0032559 | 0.0048838 |
| Case 5 | 50 | 0.0062613 | 0.0093919 |
| Case 6 | 100 | 0.0125225 | 0.0187838 |
| Case 7 | 195 | 0.0244190 | 0.0366284 |

## III. RESULTS AND DISCUSSION

### A. The Drag Coefficient

The drag coefficient of the flow surrounding the cylinder was determined through a simulation utilizing FEATool Multiphysics in MATLAB (R2019b) [23-25]. The calculation was performed using the following equations [28, 30, 31]:

$$Cd = \frac{2F_x}{\rho U_{mean}^2 D} \quad (9)$$

$$Cd = \frac{24(1+0.15Re^{0.687})}{Re} \quad (10)$$

$$Cd = \frac{5.93}{\sqrt{Re}} + 1.17 \quad (11)$$

The drag coefficient ($Cd$) and the drag force ($F_x$) were analyzed and compared to previous experimental studies [29] and Abaqus/CFD simulations [18] as well as various empirical formulas. The simulation process resulted in a set of Reynolds numbers and their corresponding drag coefficients, which were then used to create a drag curve. The drag curve depicts the relationship between the drag coefficient and Reynolds number, and can be utilized to anticipate the drag coefficient under varying flow conditions around the cylinder.

The examination of the flow around the cylinder typically revealed slightly higher drag coefficients compared to those observed in experimental studies. Despite this, the general pattern of the curve was determined to be consistent. As illustrated in Figure 6, the drag coefficient drops significantly as the Reynolds number increases from 1 to 50. Beyond this point, the decline becomes less steep and continues until $Re$ = 195. The computational study's results for Reynolds numbers from 0.1 to 1.1 were found to be relatively in line with the empirical formula for the Clift values, but as the Reynolds number increased, the results began to deviate. The discrepancy in drag coefficients between the analysis and experiment might be due to the acceleration in the lateral analysis region. When

compared to the empirical equations that predict the drag coefficient, the solution presented in [30, 31] appears to be the most thorough.

### *B. The Lift Coefficient*

The lift coefficients of hydrodynamic forces on the cylinder surface were calculated in [28]:

$$Cl = \frac{2F_y}{\rho U_{mean}^2 D} \quad (12)$$

where $Cl$ represents the coefficient of lift and $F_y$ represents the $y$-component of the lift force acting on the surface. The results of the Reynolds numbers and their respective lift coefficients can be seen in Figure 7.

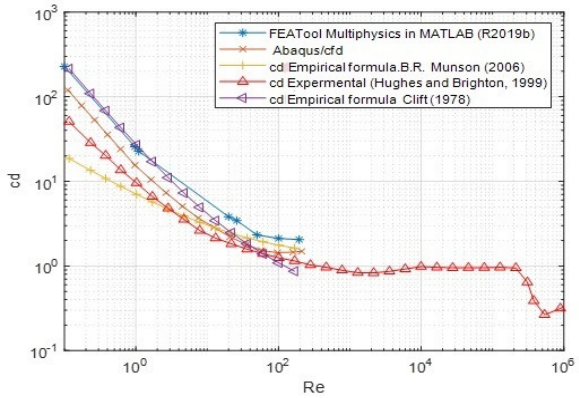


Fig. 6. Comparison of the drag coefficient as predicted by experimental studies, empirical formulas, and computational simulations, showing the variation of the coefficient with the Reynolds number.

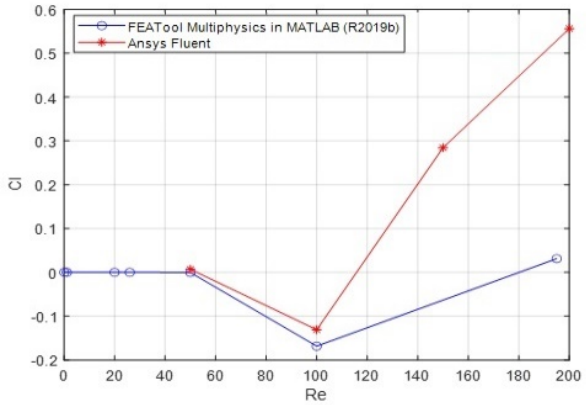


Fig. 7. Variation of the lift coefficient with the Reynolds number.

Figure 7 demonstrates that the value of $Cl$ was negligible for low Reynolds numbers (1 and 26) and became more significant for higher values (50 and 195). This is because the flow around the cylinder becomes increasingly complex and unstable as the Reynolds number increases, leading to stronger lift forces. The lift coefficient is not zero due to the existence of the Von Karman vortex street, which generates lift forces through flow fluctuations and re-circulation around the cylinder. Consequently, the lift forces operating in opposite directions in the separation region and following eddies contribute to overall lift variations ranging from negative to positive values for Reynolds numbers 50 and 100. A negative lift indicates that the force was directed downwards. When compared to the results obtained using the Ansys Fluent software [32], it was observed that the shape of the curve was similar in shape. This comparison highlights that the lift coefficients calculated through different methods are in close agreement.

### *C. Pressure Coefficient*

The pressure drag is a force that results from the difference in pressure between the front and back of a cylinder. It plays a significant role in determining the overall drag experienced by the cylinder as it moves through the fluid. To understand the pressure drag, the coefficient of pressure ($CP$) was calculated at various points on the cylinder's surface using the conformal mapping technique, as reported in [33].

$$CP = \frac{p-p_o}{1/2\rho V^2} = 1 - 4sin^2\theta \quad (13)$$

where $p$ denoted the pressure on the surface of a cylinder and the inlet pressure and the velocity in the free stream are denoted as $p_o$ and $V$, respectively, both play a role in determining the pressure distribution.

The pressure distribution on the cylinder's surface, as a function of the angle measured clockwise from the front stagnation point ($0^o$-$180^o$) is depicted in Figure 8. The illustration clearly shows that the pressure on the surface of the cylinder is at its highest near the front edge and becomes negative when the fluid flow Reynolds number surpasses 50 at angles ranging from 50 to $18^o$. As the Reynolds number increases, the minimum of the numerical curves decreases, signifying that the pressure distribution becomes increasingly intricate and diverse as the flow becomes more unstable.

The calculated pressure coefficient values were compared to those obtained through Comsol simulation, as reported in [33]. It was observed that the shape of the curve was consistent in both results. This comparison indicated a full concurrence between the two outcomes, as depicted in Figure 9.

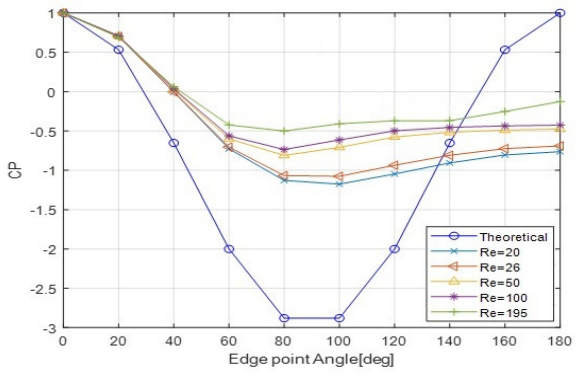


Fig. 8. At different Reynolds numbers, the pressure coefficient from the leading edge to the trailing edge of the cylinder's surface.

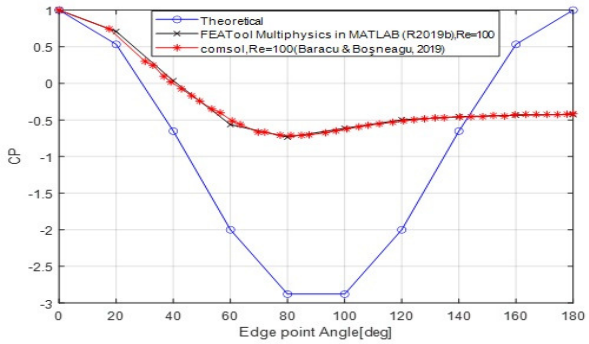


Fig. 9. At *Re* = 100, the pressure coefficient of the circular cylinder from the leading edge to the trailing edge.

### *D. The Velocity Contours*

Figure 10 presents a visual representation of the velocity distribution surrounding the cylinder. The Figure provides insight into the flow patterns and the movement of the fluid in the vicinity of the cylinder, thereby highlighting the impact of the cylinder on the surrounding flow field. This information can be used to gain a deeper understanding of the hydrodynamic forces acting on the cylinder and how these forces vary with changes in flow velocity and cylinder shape. At low Reynolds numbers (*Re* = 0.1 - 26), the velocity distribution displays a symmetrical pattern around the cylinder, demonstrating the stability and well-behaved nature of the flow. However, as the Reynolds number increases to 50 - 100, the flow becomes increasingly unstable and begins to detach from the surface of the cylinder. This is evidenced by the formation of eddies above and below the cylinder, which are a result of the flow becoming turbulent. As the turbulence intensifies, the wake behind the cylinder expands in length and the velocities above and below the cylinder become mismatched. At the highest Reynolds number (*Re* = 195), the flow becomes fully turbulent and the wake behind the cylinder becomes shorter and more energetic. This is due to the increase in the strength of the swirling flow downstream, which results in a reduction in the length of the wake past the cylinder.

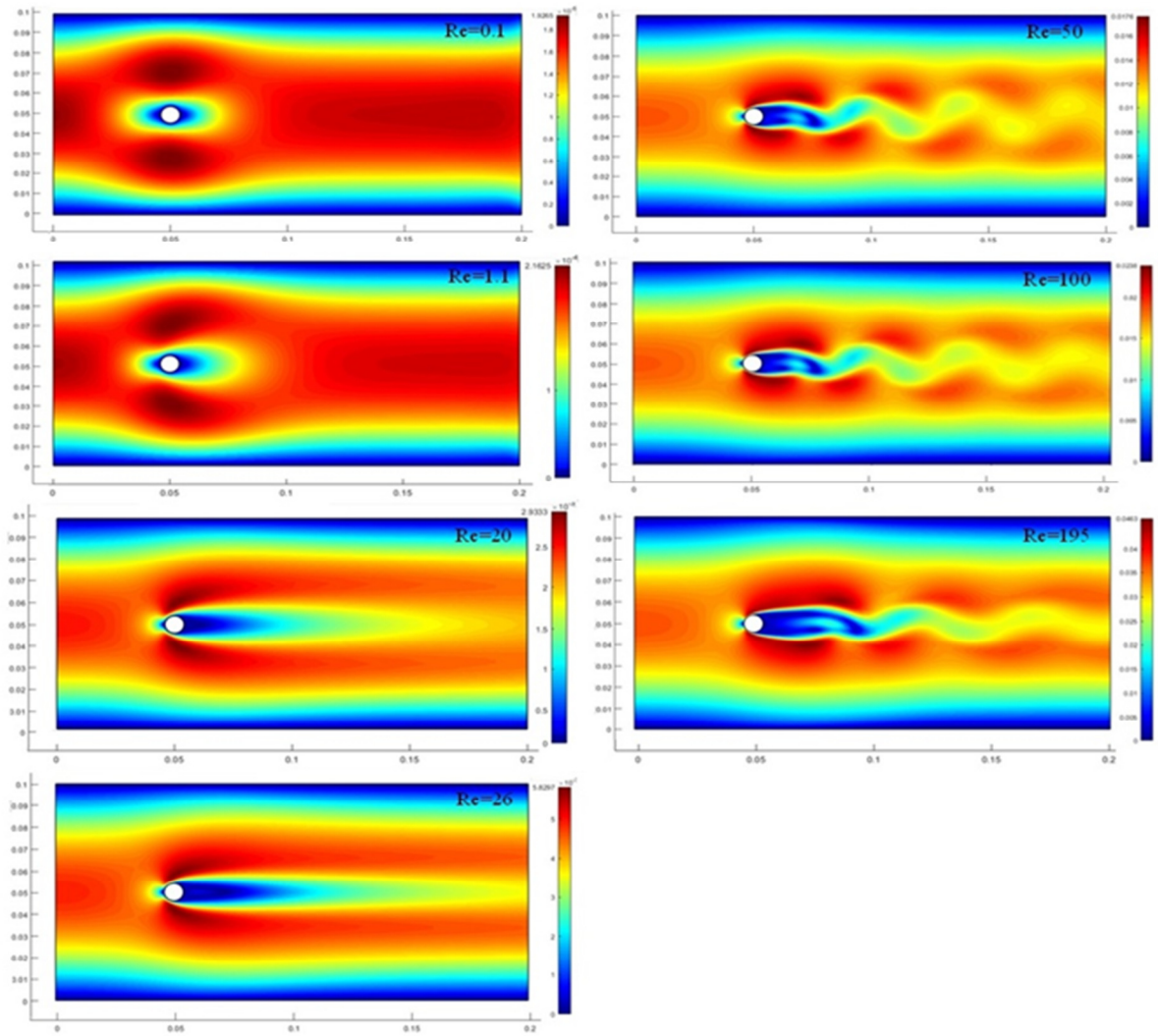


Fig. 10. Velocity contours around the cylinder.

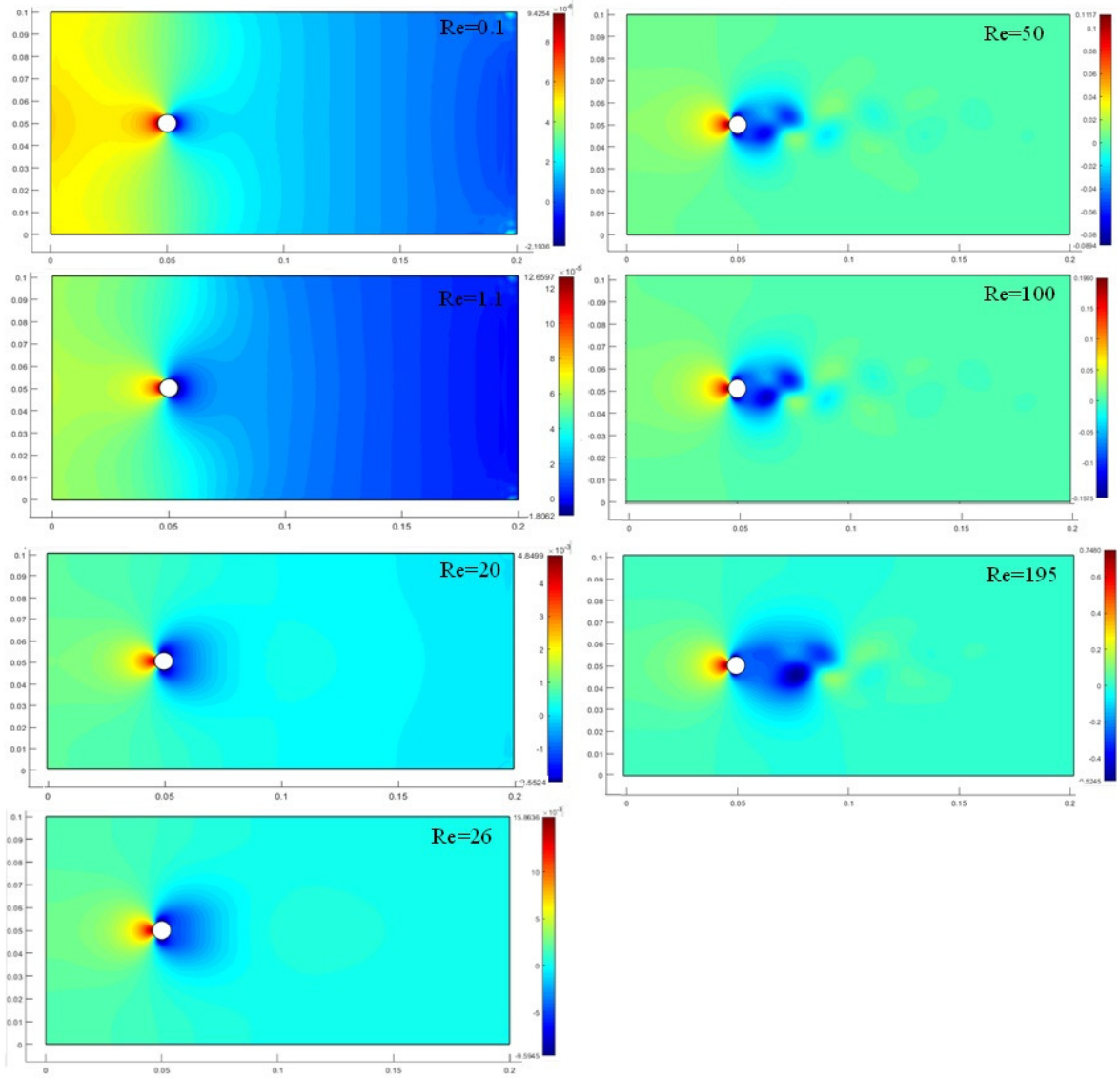


Fig. 11. Pressure distribution around the cylinder.

### *E. The Pressure Contours*

Figure 11 presents the low and high-pressure distribution surrounding the cylinder. At low Reynolds numbers, specifically *Re* = 0.1 and 1.1, the pressure is observed to be high in front of the cylinder, gradually declining as the flow moves across its surface. However, as the Reynolds number increases, the position of the low-pressure region shifts and the pressure decreases both above and below the cylinder. The wake trailing behind the cylinder becomes discernible at Reynolds numbers 50 and 100, reflecting the presence of flow separation and turbulent eddies. At the maximum Reynolds number of 195, the flow is fully turbulent, resulting in an intensified wake behind the cylinder. On the other hand, when the Reynolds number is less than 20, the flow is smooth and laminar, as indicated by the low intensity of the wake. When the Reynolds number ranges between 26 and 50, two stationary vortices are formed as the flow becomes unstable, which are attached to the top and bottom of the cylinder. As the Reynolds number continues to increase within the range of 50 to 195, the vortices that were previously attached to the top and bottom of the cylinder become detached and the vortex street is a distinctive pattern of alternating vortices that are created by the fluid flow past a cylindrical obstacle.

## IV. CONCLUSION

This study focused on analyzing the behavior of the laminar flow around a cylinder at different Reynolds numbers to predict steady-state flows in two-dimensional geometries with arbitrary obstacles. The study successfully achieved all its objectives by conducting simulations and drawing several conclusions. Firstly, the study found that the Reynolds number significantly influenced the fluid flow over a two-dimensional cylinder. The lower Reynolds numbers generated minimal or no vortex at the

back of the cylinder, while the higher Reynolds numbers resulted in a continuously oscillating vortex called the Kármán Vortex Street. This finding indicates that the fluid flow was unsteady. The computed drag coefficient results were compared with previous research, and were validated, indicating a good agreement. It was found that low Reynolds numbers resulted in larger drag coefficients, while high values produced smaller drag coefficients. Also, the study computed the lift coefficient and pressure coefficient simulation results, which were then compared to previous research, showing good agreement. Lastly, the study analyzed velocity and pressure contours, revealing that the length of the stationary vortex pair attached to the cylinder increased with an increasing Reynolds number from 50 to 195.

## REFERENCES


[1] M. Hashiguchi and K. Kuwahara, "Two-Dimensional Study of Flow past a Circular Cylinder," *Research Institute for Mathematical Sciences*, vol. 974, pp. 164–169, Nov. 1996.

[2] W. Rajhi, B. Ayadi, A. Alghamdi, and N. Messaoudene, "An Anisotropic Elastic-plastic Model for the Optimization of a Press Machine's Auxiliary Worktable Plate Thickness," *Engineering, Technology & Applied Science Research*, vol. 8, no. 2, pp. 2764–2769, Apr. 2018, https://doi.org/10.48084/etasr.1934.

[3] V. Dragan, "A Numerical Proof of Concept for Thermal Flow Control," *Engineering, Technology & Applied Science Research*, vol. 7, no. 1, pp. 1387–1390, Feb. 2017, https://doi.org/10.48084/etasr.974.

[4] I. Malael and V. Dragan, "Numerical and Experimental Efficiency Evaluation of a Counter-Rotating Vertical Axis Wind Turbine," *Engineering, Technology & Applied Science Research*, vol. 8, no. 4, pp. 3282–3286, Aug. 2018, https://doi.org/10.48084/etasr.2231.

[5] C. Wieselsberger, "New Data on the Laws of Fluid Resistance," National Aeronautics and Space Administration, NACA-TN-84, Mar. 1922.

[6] A. Roshko, "Experiments on the flow past a circular cylinder at very high Reynolds number," *Journal of Fluid Mechanics*, vol. 10, no. 3, pp. 345–356, May 1961, https://doi.org/10.1017/S0022112061000950.

[7] M. M. Zdravkovich, "A Critical Remark on Use of Drag Coefficient at Low Reynolds Numbers," 1979.

[8] P. R. Spalart, "Numerical simulation of separated flows," Ph.D. dissertation, Stanford University, Stanford, CA, USA, 1983.

[9] M. Braza, P. Chassaing, and H. H. Minh, "Numerical study and physical analysis of the pressure and velocity fields in the near wake of a circular cylinder," *Journal of Fluid Mechanics*, vol. 165, pp. 79–130, Apr. 1986, https://doi.org/10.1017/S0022112086003014.

[10] C. Liu, X. Zheng, and C. H. Sung, "Preconditioned Multigrid Methods for Unsteady Incompressible Flows," *Journal of Computational Physics*, vol. 139, no. 1, pp. 35–57, Jan. 1998, https://doi.org/10.1006/jcph.1997.5859.

[11] P. Catalano, M. Wang, G. Iaccarino, and P. Moin, "Numerical simulation of the flow around a circular cylinder at high Reynolds numbers," *International Journal of Heat and Fluid Flow*, vol. 24, no. 4, pp. 463–469, Aug. 2003, https://doi.org/10.1016/S0142-727X(03)00061-4.

[12] H. Ding, C. Shu, K. S. Yeo, and D. Xu, "Simulation of incompressible viscous flows past a circular cylinder by hybrid FD scheme and meshless least square-based finite difference method," *Computer Methods in Applied Mechanics and Engineering*, vol. 193, no. 9, pp. 727–744, Mar. 2004, https://doi.org/10.1016/j.cma.2003.11.002.

[13] M. M. Rahman, M. M. Karim, and M. A. Alim, "Numerical investigation of unsteady flow past a circular cylinder using 2-D finite volume method," *Journal of Naval Architecture and Marine Engineering*, vol. 4, no. 1, pp. 27–42, 2007, https://doi.org/10.3329/jname.v4i1.914.

[14] R. Merrick and G. Bitsuamlak, "Control of flow around a circular cylinder by the use of surface roughness: A computational and experimental approach," in *4th International Conference Advances in Wind and Structures*, Jeju, Korea, Dec. 2008, pp. 1–15.

[15] N. Rajani, A. Kandasamy, and S. Majumdar, "Numerical simulation of laminar flow past a circular cylinder," *Applied Mathematical Modelling*, vol. 33, no. 3, pp. 1228–1247, Mar. 2009, https://doi.org/10.1016/j.apm.2008.01.017.

[16] N. Kanaris, D. Grigoriadis, and S. Kassinos, "Three dimensional flow around a circular cylinder confined in a plane channel," *Physics of Fluids*, vol. 23, no. 6, Jun. 2011, Art. no. 064106, https://doi.org/10.1063/1.3599703.

[17] R. Farhoud, S. Amiralaie, G. Jabbari, and S. Amiralaie, "Numerical Study of Unsteady Laminar Flow around a Circular Cylinder," *Journal of Civil Engineering and Urbanism*, vol. 2, no. 2, pp. 63–67, Jan. 2012.

[18] M. Sato and T. Kobayashi, "A fundamental study of the flow past a circular cylinder using Abaqus/CFD," in *SIMULIA Community Conference*, Providence, RI, USA, Dec. 2012, pp. 1–15.

[19] Y. Bao, D. Zhou, and J. Tu, "Flow characteristics of two in-phase oscillating cylinders in side-by-side arrangement," *Computers & Fluids*, vol. 71, pp. 124–145, Jan. 2013, https://doi.org/10.1016/j.compfluid.2012.10.013.

[20] D. E. Rival, J. Kriegseis, P. Schaub, A. Widmann, and C. Tropea, "Characteristic length scales for vortex detachment on plunging profiles with varying leading-edge geometry," *Experiments in Fluids*, vol. 55, no. 1, Jan. 2014, Art. no. 1660, https://doi.org/10.1007/s00348-013-1660-x.

[21] J. MacArthur, "Wall shear-stress management on an accelerating circular cylinder," M.S. thesis, The University of New Brunswick, 2017.

[22] V. Ageorges, J. Peixinho, G. Perret, G. Lartigue, and V. Moureau, "Numerical and experimental studies of the flow around a partially submerged vertical cylinder," in *24th French Congress of Mechanics*, Brest, France, Aug. 2019, pp. 1–10.

[23] N. Chakraborty, *Simulation of Flow past a Cylinder at Moderate Reynolds Numbers (CFD)*. London, UK: University of London, 2021.

[24] A. Samanta, "Simulation of flows with different shaped cylinders using CFD," *American Journal of Applied Mathematics and Computing*, vol. 2, no. 1, pp. 19–24, 2022.

[25] M. Ghalandari, E. Mirzadeh Koohshahi, F. Mohamadian, S. Shamshirband, and K. W. Chau, "Numerical simulation of nanofluid flow inside a root canal," *Engineering Applications of Computational Fluid Mechanics*, vol. 13, no. 1, pp. 254–264, Jan. 2019, https://doi.org/10.1080/19942060.2019.1578696.

[26] V. John and G. Matthies, "Higher-order finite element discretizations in a benchmark problem for incompressible flows," *International Journal for Numerical Methods in Fluids*, vol. 37, no. 8, pp. 885–903, 2001, https://doi.org/10.1002/fld.195.

[27] R. Rannacher and G. Wittum, *On high order methods for the stationary incompressible Navier-Stokes equations*. 1998.

[28] D.-W. Sun and B.-X. Sun, "The Research on Flow Past a Cylinder," in *3rd Annual International Conference on Mechanics and Mechanical Engineering*, Chengdu, China, Dec. 2016, pp. 1047–1050, https://doi.org/10.2991/mme-16.2017.149.

[29] D. D. Gray, *A First Course in Fluid Mechanics for Civil Engineers*. Highlands Ranch, CO, USA: Water Resources Publication, 1999.

[30] R. Clift, J. R. Grace, and M. E. Weber, "Formation and breakup of fluid particles," in *Bubbles, Drops and Particles*, New York, NY, USA: Academic Press, 1978, pp. 321–351.

[31] B. R. Munson, D. F. Young, and T. H. Okiishi, *Fundamentals of Fluid Mechanics*. New York, NY, USA: Wiley, 2005.

[32] "To simulate flow over a cylinder and explain the phenomenon of Karmen vortex street using Ansys Fluent." https://skill-lync.com/student-projects/Steady-Vs-Unsteady-flow-over-a-cylinder-59295.

[33] T. Baracu and R. Bosneagu, "Numerical analysis of the flow around a cylinder for the perspective of correlations of the drag coefficient of the ship's hulls," *Scientific Bulletin of Naval Academy*, vol. 22, no. 2, pp. 256–267, 2019, https://doi.org/10.21279/1454-864X-19-I2-031.